Geophysical Research Letters

RESEARCH LETTER
10.1029/2019GL082095

Key Points:
- Three types of whistler mode waves are observed during conjunction events between Van Allen Probes and POES/MetOp
- These whistler mode waves include plume whistler mode waves, plasmaspheric hiss, and exohiss
- Plume whistler mode waves are very effective in producing energetic electron precipitation (from tens to hundreds of keV)

Supporting Information:
- Supporting Information S1

Correspondence to:
W. Li,
wenli77@bu.edu

Citation:
Li, W., Shen, X.-C., Ma, Q., Capannolo, L., Shi, R., Redmon, R. J., et al. (2019). Quantification of energetic Electron precipitation driven by plume whistler mode waves, Plasmaspheric hiss, and exohiss. *Geophysical Research Letters*, *46*, 3615–3624. https://doi.org/10.1029/2019GL082095

Received 16 JAN 2019
Accepted 4 MAR 2019
Accepted article online 11 MAR 2019
Published online 8 APR 2019

Quantification of Energetic Electron Precipitation Driven by Plume Whistler Mode Waves, Plasmaspheric Hiss, and Exohiss

W. Li[1], X.-C. Shen[1], Q. Ma[1,2], L. Capannolo[1], R. Shi[1], R. J. Redmon[3], J. V. Rodriguez[3,4], G. D. Reeves[5], C. A. Kletzing[6], W. S. Kurth[6], and G. B. Hospodarsky[6]

[1]Center for Space Physics, Boston University, Boston, MA, USA, [2]Department of Atmospheric and Oceanic Sciences, University of California, Los Angeles, CA, USA, [3]National Centers for Environmental Information, NOAA, Boulder, CO, USA, [4]Cooperative Institute for Research in Environmental Sciences, University of Colorado Boulder, Boulder, CO, USA, [5]Space Science and Applications Group, Los Alamos National Laboratory, Los Alamos, NM, USA, [6]Department of Physics and Astronomy, University of Iowa, Iowa City, IA, USA

Abstract Whistler mode waves are important for precipitating energetic electrons into Earth's upper atmosphere, while the quantitative effect of each type of whistler mode wave on electron precipitation is not well understood. In this letter, we evaluate energetic electron precipitation driven by three types of whistler mode waves: plume whistler mode waves, plasmaspheric hiss, and exohiss observed outside the plasmapause. By quantitatively analyzing three conjunction events between Van Allen Probes and POES/MetOp satellites, together with quasi-linear calculation, we found that plume whistler mode waves are most effective in pitch angle scattering loss, particularly for the electrons from tens to hundreds of keV. Our new finding provides the first direct evidence of effective pitch angle scattering driven by plume whistler mode waves and is critical for understanding energetic electron loss process in the inner magnetosphere. We suggest the effect of plume whistler mode waves be accurately incorporated into future radiation belt modeling.

Plain Language Summary Electron precipitation into Earth's upper atmosphere is an important loss mechanism of energetic electrons trapped in the inner magnetosphere. Although whistler mode waves are known to be effective in producing electron precipitation through pitch angle scattering, the relative roles of various whistler mode waves that play in electron losses are unclear. In this letter, we quantitatively analyze conjunction events, where Van Allen Probes observed various whistler mode waves near the equator and Low-Earth-Orbiting satellites detected electron precipitation approximately along the same magnetic field line but at low altitudes. By combining the satellite data analysis and quasi-linear theory, we found that whistler mode waves observed in plumes are very effective in scattering energetic electrons, which are ultimately lost through interacting with the neutral atmosphere. Our new finding provides the direct evidence that plume whistler mode waves play an important role in energetic electron precipitation, which is crucial for understanding energetic electron loss process in the Earth's inner magnetosphere.

1. Introduction

Various types of whistler mode waves are present in the Earth's inner magnetosphere, including hiss observed inside the plasmasphere (e.g., Thorne et al., 1973), whistler mode waves in plasmaspheric plumes (called plume whistler mode waves hereafter; Chan & Holzer, 1976; Su et al., 2018; Woodroffe et al., 2017), chorus waves observed outside the plasmapause (e.g., Burtis & Helliwell, 1969; Koons & Roeder, 1990), and exohiss observed in the plasmatrough (Thorne et al., 1973; Zhu et al., 2015). Typical properties and generation mechanisms of plasmaspheric hiss, chorus, and exohiss, as well as their scattering effects on energetic electrons, have been extensively studied over the past several decades (e.g., Bortnik, Thorne, Meredith, 2008; Horne et al., 2005; Li, Thorne, et al., 2013; Omura et al., 2008; Santolík et al., 2003; Thorne et al., 1973, 2013; Zhu et al., 2015), while our understanding of plume whistler mode waves is rather limited.

Plasmaspheric plumes consist of plasma being drained from the reservoir of plasmaspheric plasma and extending into the more tenuous outer magnetosphere (Carpenter et al., 1993; Chen & Wolf, 1972; Elphic

et al., 1996; Goldstein et al., 2004; Grebowsky, 1970; Weiss et al., 1997) and are often associated with large density fluctuations (Borovsky & Denton, 2008; Goldstein et al., 2004; Moldwin et al., 2004; Spasojević et al., 2003). Plasma waves in plumes are particularly interesting, because a plume is a unique region where total plasma density is typically high, but energetic particles (>tens keV) are accessible, thus providing favorable conditions for various types of wave generation (Chan & Holzer, 1976; Hayakawa et al., 1986; Ma et al., 2014; Tsurutani et al., 2015; Usanova et al., 2013; Woodroffe et al., 2017). Recently, plume whistler mode waves are found to sometimes exhibit discrete rising tones (e.g., Su et al., 2018), which are somewhat similar to typical chorus waves (Li et al., 2011; Santolík et al., 2003). This discrete feature is different from typical plasmaspheric hiss that exhibits incoherent broadband emissions (e.g., Bortnik, Thorne, & Meredith, 2008; Santolik et al., 2001; Thorne et al., 1973) and could potentially lead to nonlinear interactions between waves and electrons (e.g., Albert, 2002; Bortnik, Thorne, Inan, 2008; Tao et al., 2014). Moreover, Su et al. (2018) reported that plume whistler mode waves could have an unexpectedly large amplitude (~1.5 nT) and suggested that these waves were locally generated probably through a combination of linear and nonlinear instabilities of hot electrons.

Plasmaspheric plumes are found to be favorable for enhancing pitch angle scattering of radiation belt electrons, thus leading to electron precipitation into the upper atmosphere (Borovsky et al., 2014; Summers et al., 2008; Zhang et al., 2018). Borovsky and Steinberg (2006) found that relativistic electron dropouts at geosynchronous orbit often coincided with the presence of plasmaspheric plumes, suggesting the potential loss of energetic electrons due to interactions with the enhanced plasma waves in plumes. Furthermore, Summers et al. (2008) evaluated electron precipitation loss due to plume whistler mode waves by analyzing 14 representative plumes and found that pitch angle scattering by plume whistler mode waves can be efficient for inducing precipitation loss of radiation belt electrons with energy from 100 keV to 1 MeV, though the loss rates are highly dependent on wave power, L shell, and electron energy.

Despite the potential importance of plume whistler mode waves in electron scattering, the direct evidence showing energetic electron precipitation driven by plume whistler mode waves is still lacking. In this letter, by analyzing fortuitous conjunction events between near-equatorial satellites (Van Allen Probes) and Low-Earth-Orbiting satellites (POES/MetOp), we quantitatively evaluate and compare the energetic electron precipitation driven by three types of whistler mode waves: (1) plume whistler mode waves, (2) plasmaspheric hiss, and (3) exohiss. Moreover, using quasi-linear theory we estimate electron precipitations caused by these three types of whistler mode waves based on the observed wave and plasma properties and compare them with the POES/MetOp measurements.

2. Overview of Conjunction Events Between Van Allen Probes and POES/MetOp

Figures 1–3 show an overview of conjunction events between the twin Van Allen Probes orbiting near the equator (Mauk et al., 2013) and POES/MetOp orbiting at a low altitude of ~800 km approximately along the same magnetic field line (Evans & Greer, 2004). This event occurred during a relatively quiet period (2 September 2013), when Sym-H remained above −30 nT over the preceding 2 days, but there was a modest substorm over 16–20 UT with a minimum AL index of ~ −400 nT (not shown). Figure 1 shows the total electron density and wave observation from Van Allen Probe A (left) and B (right) measured by the EMFISIS Waves instrument (Kletzing et al., 2013) onboard Van Allen Probes. Total electron density (Figures 1a and 1h) was inferred from the upper hybrid resonance line (Kurth et al., 2015) and was used to identify various regions: (1) plume (magenta), (2) plasmasphere (blue), and (3) plasmatrough (green). A plasmapause location (indicated by the vertical black line in Figure 1) is defined as the innermost steep density gradient; more specifically, a factor of ~5 drop within 0.5 L (Moldwin et al., 2002). After a plasmapause is identified, a plume is defined in a region outside the plasmapause, where plasma density is considerably larger than the plasmatrough density at lower L shells. Based on the plasma density and wave polarization properties (Figures 1d, 1e, 1k, and 1l), five different types of plasma waves were identified (see the detailed criteria in Table S1 in the supporting information) with the wave flag shown in Figures 1f and 1m, namely, plasmaspheric hiss (yellow), exohiss (green), plume whistler mode wave (orange), chorus (cyan), and magnetosonic waves (red). Over 15:30–20:30 UT, Van Allen Probe A (Figures 1b–1f) first observed magnetosonic waves and weak exohiss in the plasmatrough (15:30–16:00 UT), strong whistler mode waves in plasmaspheric plumes (16:00–18:30 UT), magnetosonic waves in the

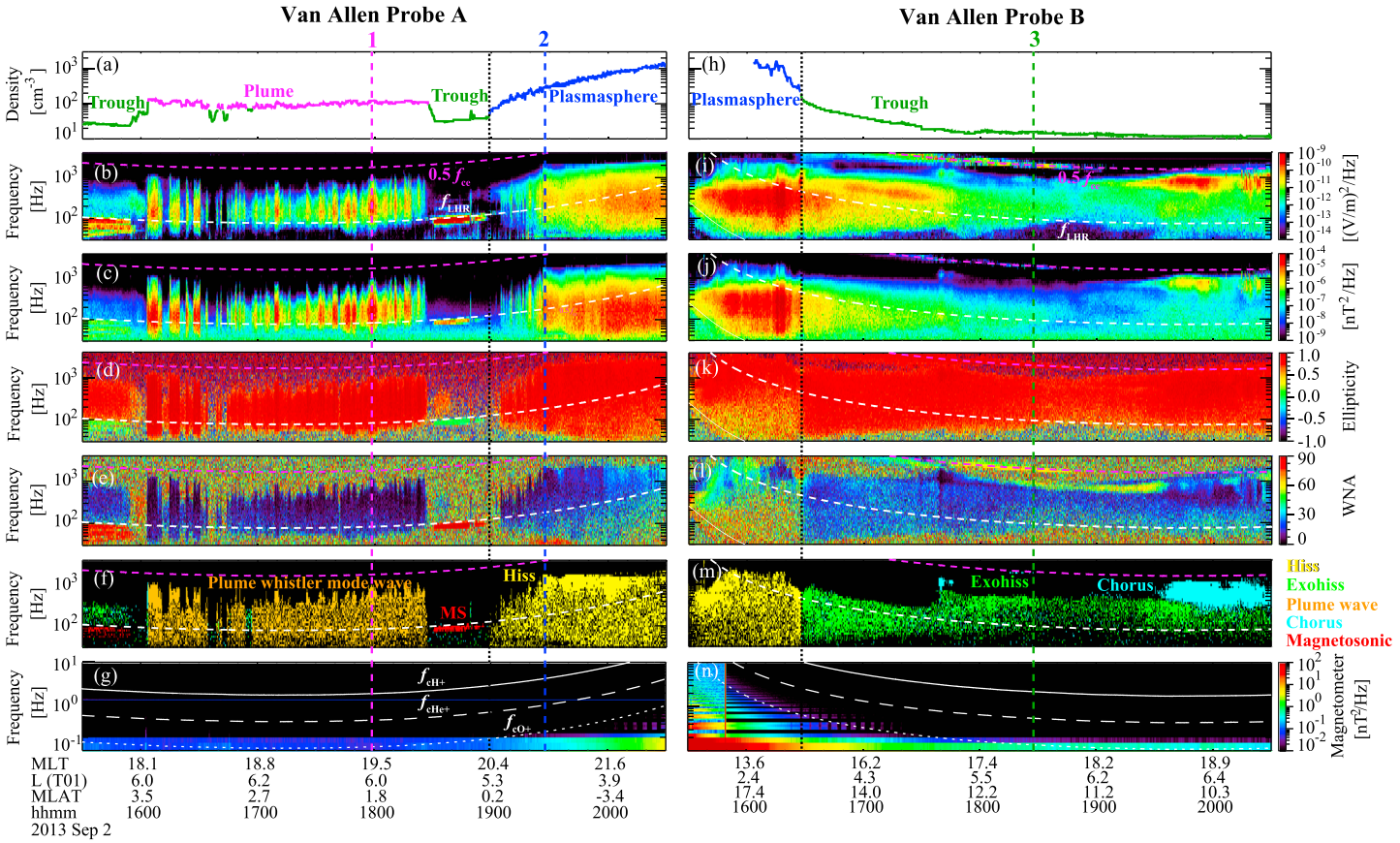

Figure 1. Overview of the observation from Van Allen Probe A and B on 2 September 2013. (a) Total electron density inferred from the upper hybrid resonance line, where the magenta, blue, and green lines represent the regions of plume, plasmasphere, and plasmatrough respectively. (b) Frequency-time spectrogram of electric spectral density, (c) magnetic spectral density, (d) ellipticity, (e) wave normal angle (WNA), and (f) wave flag color-coded for different types of magnetospheric waves. In panels (b)–(f), the magenta (white) dashed line represents 0.5 f_{ce} (f_{LHR}), where f_{ce} (f_{LHR}) is electron cyclotron frequency (lower hybrid resonance frequency). (g) Frequency-time spectrogram of magnetic spectral density from the magnetometer data, where the solid, dashed, and dotted lines indicate proton, helium, and oxygen cyclotron frequency. (h–n) Similar to panels (a)–(g) but observed by Van Allen Probe B over the same time period. The black dotted vertical lines at ~19 UT on the left panels and ~16:30 UT on the right panels represent the plasmapause crossing. The magenta (Time 1), blue (Time 2), and green vertical lines (Time 3) indicate the conjunction time with POES/MetOp.

plasmatrough again (18:30–19:00 UT), and hiss inside the plasmasphere (after ~19 UT). Simultaneously, Van Allen Probe B (Figures 1i–1m) detected hiss inside the plasmasphere (before ~16:30 UT), as well as weak exohiss below 1 kHz and very weak chorus waves with frequencies near 0.5 f_{ce} in the plasmatrough region (~16:30–19:00 UT), without detecting any plumes. Since exohiss is suggested to be formed due to the leakage of plasmaspheric hiss (Thorne et al., 1973; Zhu et al., 2015), its amplitude is typically weaker than that of plasmaspheric hiss. After ~19 UT quasi-parallel chorus waves with modest wave amplitudes (from ~16 to ~42 pT) were detected at L shells above ~6.2. It is worthwhile to note that we adopted the L shell based on the T01 magnetic field model (Tsyganenko, 2002), since the in situ magnetic field measurements from Van Allen Probes were closest to the magnetic field values from the T01 magnetic field model among all available Tsyganenko magnetic field models. Figure 2 illustrates the trajectories of Van Allen Probe A and B over 15:30–20:30 UT on 2 September 2013 color coded for the different regions. The structure of the plasmasphere and plume regions is depicted based on the plasma density observation from Van Allen Probes. It is important to note that Van Allen Probe B, which did not detect any plume features, was traveling in an earlier magnetic local time (over 13–18 MLT) than Van Allen Probe A (over ~18–22 MLT), which clearly detected a plume. Interestingly, the observed plume whistler mode waves (Figures 1b and 1c) were intense (~120 pT) and exhibited strong modulation, probably due to the modulating plasma density (e.g., Chen et al., 2012). High-resolution waveform data were available for the observed plume whistler mode waves during several short intervals (6 s) over the period of 16:00–18:30

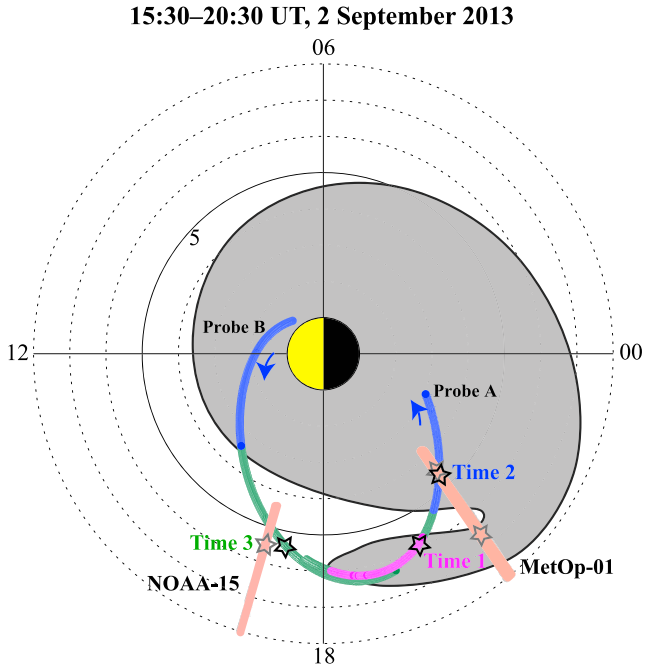

Figure 2. A cartoon illustrating the trajectories of Van Allen Probes and POES/MetOp satellites over 15:30–20:30 UT on 2 September 2013. The gray-shaded region represents the plasmasphere and plume with the black solid line indicating the boundary. The color-coded curves along the Van Allen Probes trajectory indicate plasmasphere (blue), plasmatrough (green), and plume (magenta). The light red lines represent the trajectories of NOAA-15 and MetOp-01. The gray (black) star symbol indicates the location of POES/MetOp (Van Allen Probes) when the conjunction occurred at Times 1, 2, and 3.

UT, and they all exhibited broadband hiss-like emissions rather than discrete rising or falling tone elements (not shown). It is also worth noting that electromagnetic ion cyclotron (EMIC) waves, which are sometimes observed in plumes (e.g., Usanova et al., 2013), were not detected by Van Allen Probe A or B over the entire time period of 15:30–20:30 UT (Figures 1g and 1n).

Around Times 1, 2, and 3, as marked by the vertical lines in Figure 1, POES/MetOp satellites passed through the magnetically conjugate region at a low altitude (~800 km). Figure 3 shows the electron flux observation from POES/MetOp around the conjunction Times 1, 2, and 3. The particle detector onboard POES/MetOp has two telescopes with the 0° (90°) telescope measuring precipitating (trapped or quasi-trapped) electrons at various energies of ≳30, ≳100, and ≳300 keV (Evans & Greer, 2004; Green, 2013). A proton channel (≳6.9 MeV) mainly detects electrons above ≳700 keV and thus can be used to monitor highly relativistic electrons (Green, 2013; Rodger et al., 2010; Yando et al., 2011). Proton contamination at ≳30 , ≳100, and ≳300 keV channels was removed using the method described in Peck et al. (2015). During Time 1 (~18:07 UT; Figures 3a and 3b), MetOp-01 traversed through ~20.8 MLT and detected strong electron precipitation in energy channels of ≳30, ≳100, and approximately ≳300 keV over *L* shells of 6.8–7.5 (6.1–6.6) based on the T01 (International Geomagnetic Reference Field) magnetic field model, where the precipitating electron flux was close to the trapped value. The gray-shaded region in Figure 3b, also marked with the gray star symbol in Figure 2, is roughly in the conjugate location with the region where plume whistler mode waves were detected by Van Allen Probe A (marked with the black star symbol in Figure 2). During Time 2 (~19:47 UT; Figures 3c and 3d), ~100 min after Time 1, MetOp-01 passed through the same *L* shell range at ~20.8 MLT again. In particular, near the

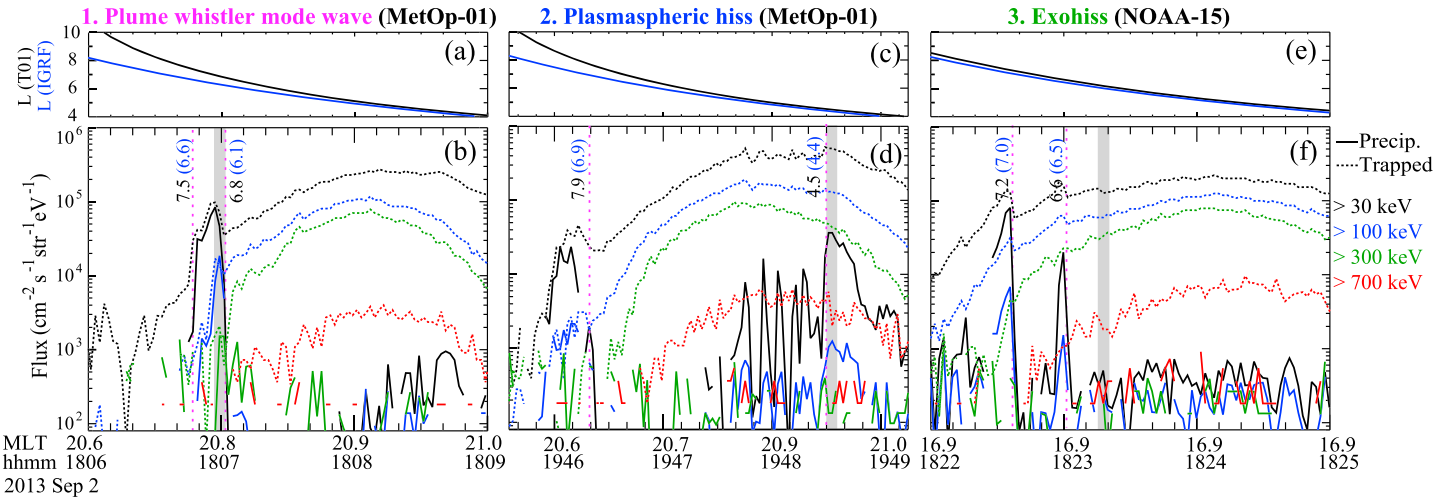

Figure 3. POES/MetOp observation of energetic electron precipitation during the three conjunction intervals (Time 1: plume whistler mode waves; Time 2: plasmaspheric hiss; Time 3: exohiss). (a) *L* shells of MetOp-01 based on the T01 (black) and IGRF (blue) magnetic field model during Time 1. (b) Precipitating (solid lines) and trapped or quasi-trapped (dotted lines) electron fluxes at ≳30 (black), ≳100 (blue), ≳300 (green), and ≳700 keV (red). In panel (b), the gray-shaded region represents the *L* shell range of the rough conjunction with Van Allen Probe A, and the magenta dotted vertical lines indicate the precipitation boundaries, where the corresponding *L* shell from the T01 (IGRF) magnetic field model is indicated with the black (blue) text. (c and d) Similar to (a) and (b) but at ~19:47 UT (~100 min later) observed by MetOp-01. (e and f) Similar to (a) and (b) but at ~18:23 UT observed by NOAA-15.

conjunction region (gray-shaded region in Figure 3d) with Van Allen Probe A, MetOp-01 detected modest electron precipitation at ≳30 and ≳100 keV. The strong electron precipitation at ≳30 and ≳100 keV at L(T01) > 7.9 and L (IGRF) > 6.9 in Figure 3d at ~19:46 UT might still be caused by the plume whistler mode waves, which may have lasted for at least a few hours, although the conjugate wave measurements near the equator were not available to verify it. This feature of long-lasting plume whistler mode waves is also supported by the fact that NOAA-16 also observed very similar electron precipitation (not shown) to that by MetOp-01 (Figure 3b) but at ~18:52 UT, which occurred between Times 1 and 2 at a slightly earlier MLT (~20.4). During Time 3 (~18:23 UT; Figures 3e and 3f), NOAA-15 passed through the L shell from 9 to 4 at ~17 MLT. Near the conjugate region (gray shaded region in Figure 3f) with Van Allen Probe B, which observed very weak exohiss, NOAA-15 detected little electron precipitation at all energy channels (≳30, ≳100, ≳300, and ≳700 keV). The relatively strong electron precipitation near L(T01) ~ 6.6 and L(T01) ~ 7.2 (magenta dotted vertical lines) might be caused by chorus waves, since modest chorus waves were present at L(T01) > 6, as observed by Van Allen Probe B, but after ~19:30 UT (~1 h later). It is worth noting that there was no clear correlation between the observed electron and proton precipitation at Times 1, 2, and 3 (not shown), supporting that the observed electron precipitations near conjunction were not caused by EMIC waves. The electron observations at Times 1, 2, and 3 indicate that the relatively strong plume whistler mode waves led to the observed strong electron precipitation at Time 1, the modest plasmaspheric hiss drove the modest electron precipitation at Time 2, and the weak exohiss caused little electron precipitation at Time 3. The quantitative calculation of electron precipitation driven by the above three types of whistler mode waves is discussed in section 3.

3. Calculation of Electron Precipitation Based on Quasi-linear Theory

We used quasi-linear theory to calculate the electron precipitation driven by plume whistler mode waves, plasmaspheric hiss, and exohiss. The Full Diffusion Code (Ni et al., 2008) is used to calculate bounce-averaged pitch angle diffusion coefficients of three types of whistler mode waves based on the observed wave and plasma properties, as listed in Table S2. We adopted the observed wave frequency spectra for each type of whistler mode waves to calculate diffusion coefficients by including Landau resonance and cyclotron resonances with resonance harmonics from −10 to +10. Wave normal angles of plume whistler mode waves, plasmaspheric hiss, and exohiss are assumed to be quasi-parallel near the equator, which is consistent with the in situ Van Allen Probes observation (Figures 1e and 1l), and become more oblique with increasing magnetic latitudes (Ni et al., 2013).

Figures 4a–4c show the bounce-averaged pitch angle diffusion coefficients for the plume whistler mode waves observed at Time 1, plasmaspheric hiss detected at Time 2, and exohiss measured at Time 3. The amplitude of the plume whistler mode wave is the strongest (120 pT), plasmaspheric hiss is modestly strong (74 pT), but exohiss is very weak (9 pT). As a consequence, pitch angle diffusion coefficients of plume whistler mode waves are largest on a timescale down to ~10 min at ~10 keV, whereas pitch angle diffusion coefficients of exohiss are extremely small on a timescale of tens of hours at ~10 keV. The ratio between the plasma frequency and electron cyclotron frequency (f_{pe}/f_{ce}) is largest for plume whistler mode waves (28.1), modest for plasmaspheric hiss (~19.7), and smallest for exohiss (~8.8). As a consequence, the energy of electrons (Figures 4a–4c), which are subject to strongest pitch angle scattering near the loss cone, tends to increase with decreasing f_{pe}/f_{ce} (<10 keV for plume whistler mode waves, ~25 keV for plasmaspheirc hiss, and ~100 keV for exohiss). Figures 4d–4f show the direct comparison between pitch angle diffusion coefficients near the loss cone ($D_{\alpha\alpha}|_{LC}$) and strong diffusion limit (D_{SD}; Summers & Thorne, 2003) for three types of whistler mode waves, respectively. $D_{\alpha\alpha}|_{LC}$ is closest to D_{SD} for plume whistler mode waves (particularly at a few tens of keV), while $D_{\alpha\alpha}|_{LC}$ is more than an (2) order(s) of magnitude smaller than D_{SD} for plasmaspheric hiss (exohiss). Moreover, we use the pitch angle diffusion coefficients to infer the electron pitch angle distributions in a quasi-equilibrium state (Kennel & Petschek, 1966; Li, Ni, et al., 2013; Ni et al., 2014; Theodoridis & Paolini, 1967). This approach is reasonable to estimate wave-driven electron precipitations, since these whistler mode waves typically last longer than several minutes (as an example shown in Figure 1) and the 1-D Fokker-Planck simulation result (not shown) indicates that electron pitch angle distribution near the loss cone (equatorial pitch angles over 0–10°) reaches a quasi-steady state within a few minutes after interacting with these whistler mode waves. The bottom panels in Figure 4 show the normalized electron flux (to the flux value at 90° pitch angle) as a function of equatorial pitch angle color coded for

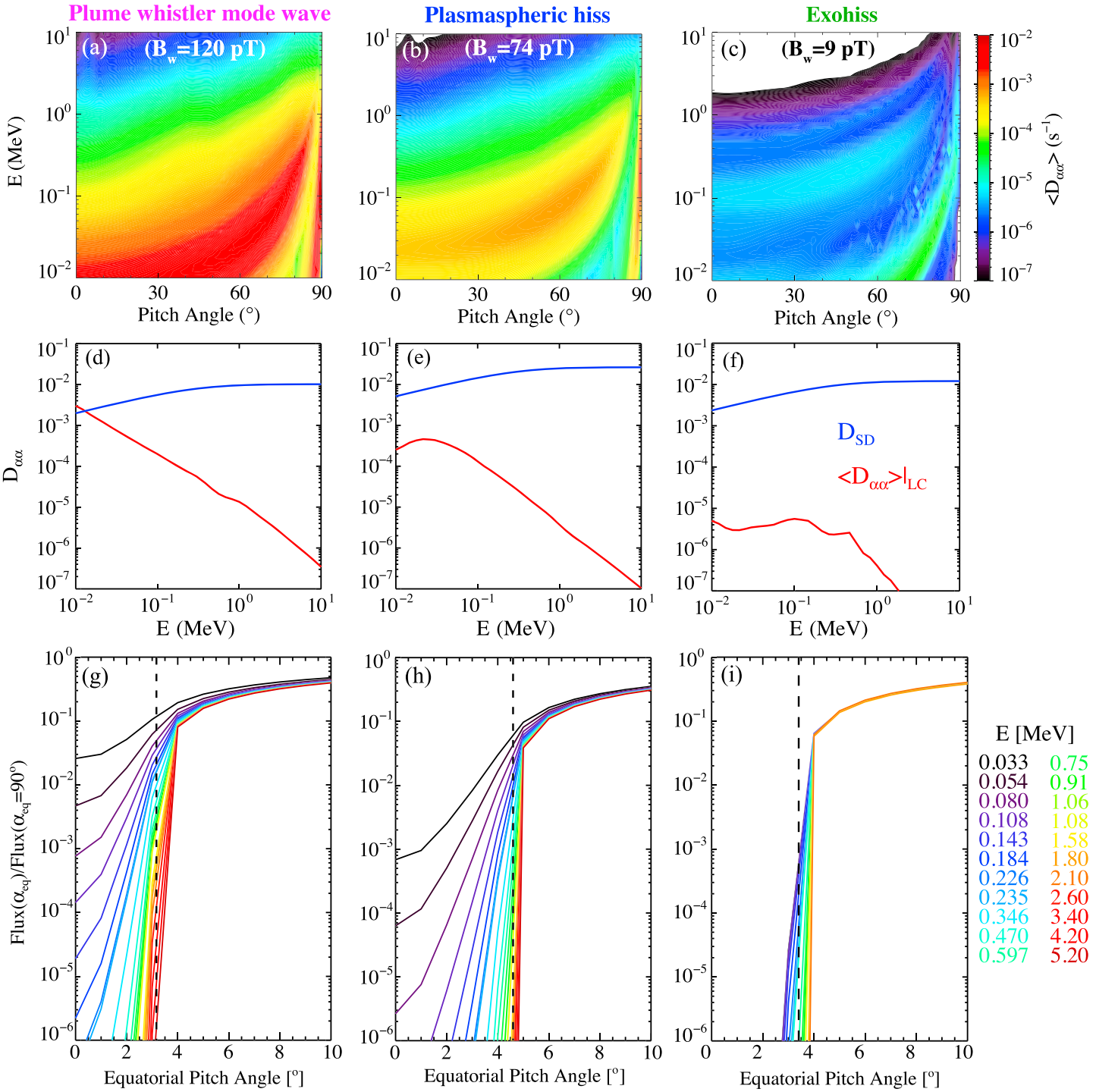

Figure 4. Calculated electron precipitation based on quasi-linear theory driven by (left) plume whistler mode waves, (middle) plasmaspheric hiss, and (right) exohiss. Bounce-averaged pitch angle diffusion coefficients as a function of equatorial pitch angle and energy due to plume whistler mode waves (Figure 4a), plasmaspheric hiss (Figure 4b), and exohiss (Figure 4c). The comparison between pitch angle diffusion coefficients near the loss cone (red lines) and strong diffusion limit (blue lines) at the location where plume whistler mode waves (Figure 4d), plasmaspheric hiss (Figure 4e), and exohiss (Figure 4f) were observed. Normalized electron flux to the 90° value as a function of equatorial pitch angle color-coded for various energies from ~30 keV to 5.2 MeV driven by plume whistler mode waves (Figure 4g), plasmaspheric hiss (Figure 4h), and exohiss (Figure 4i). The black vertical dashed lines on the bottom panels represent the corresponding equatorial bounce loss cone.

various energies. Among three types of whistler mode waves, the loss cone is most filled for the plume whistler mode waves, modestly filled for the plasmaspheric hiss, but mostly empty for the exohiss. The trend shown in Figures 4d–4i is consistent with the POES/MetOp observation, where the ratio of precipitating-to-trapped electrons is highest for plume whistler mode waves, modest for plasmaspheric hiss, and lowest for exohiss.

4. Summary and Discussion

In this letter, we report fortuitous conjunction events between Van Allen Probes and POES/MetOp satellites and quantitatively evaluate and directly compare energetic electron precipitation driven by plume whistler mode waves, plasmaspheric hiss, and exohiss. Most importantly, we provide the first direct evidence of efficient electron precipitation from tens to hundreds of keV driven by plume whistler mode waves. The principal findings of this study are summarized below.

1. During a modest substorm activity, a plasmaspheric plume was present over the dusk-to-premidnight sector. Van Allen Probe A, which traversed the postdusk sector, observed whistler mode waves in plumes and hiss inside the plasmasphere, whereas Van Allen Probe B, which traveled through the predusk sector, observed exohiss outside the plasmapause and chorus at high L shells (>6.2) without detecting any plume features.
2. In these conjunction events, plume whistler mode waves were strongest (~120 pT), plasmaspheric hiss was modestly strong (~74 pT), and exohiss was very weak (~9 pT). The wave normal angles of all three types of whistler mode waves were quasi-parallel near the equator. Moreover, during the entire conjunction interval EMIC waves were not detected by Van Allen Probes.
3. In the conjugate location at low altitudes, POES/MetOp detected strongest electron precipitation at $\gtrsim$30, $\gtrsim$100, and $\gtrsim$300 keV in association with the plume whistler mode waves, modest electron precipitation at $\gtrsim$30 and $\gtrsim$100 keV in association with the plasmaspheric hiss, but little electron precipitation corresponding to the exohiss.
4. The trend of the estimated electron precipitation using quasi-linear theory based on the observed wave and plasma parameters is consistent with the POES/MetOp observation, clearly indicating that plume whistler mode waves are most effective in producing energetic electron precipitation from tens to hundreds of keV compared to the plasmaspheric hiss and the exohiss in this event.

This letter presents a pilot study showing the direct evidence of efficient pitch angle scattering driven by plume whistler mode waves through analyzing fortuitous conjunction events, where plume whistler mode waves were observed to be strong (~120 pT) in association with a modest substorm activity and exhibit hiss-like emissions. A recent study by Shi et al. (2019) analyzed several years of Van Allen Probes wave data and found that plume whistler mode waves are typically stronger (up to a few hundred pT) than plasmaspheric hiss, and their occurrence rate could be up to a few tens of %, particularly during geomagnetically active periods. However, the detailed emission structures were not analyzed systematically in Shi et al. (2019), since they used the survey-mode wave data. Moreover, Su et al. (2018) reported plume whistler mode waves with very large amplitudes (~1.5 nT) and rising tone elements embedded on top of hiss-like emissions. It would be very interesting to understand how the detailed emission structures of plume whistler mode waves (rising/falling tones or hiss-like emissions) vary under various geomagnetic activities. A more systematic study through analyzing a sufficient number of high-resolution waveform data for plume whistler mode waves, although beyond the scope of the present pilot study, is needed to address this interesting question and is left for future investigations.

Our new findings on the efficient pitch angle scattering caused by plume whistler mode waves, together with their relatively strong wave amplitudes compared to plasmaspheric hiss from the statistical results by Shi et al. (2019), indicate their potential importance in the loss process of energetic electrons in the Earth's inner magnetosphere. It is worthwhile to note that plume whistler mode waves are typically observed in the region with relatively high values of f_{pe}/f_{ce}, thus are particularly effective in driving pitch angle scattering loss of electrons with lower energy compared to plasmaspheric hiss and exohiss. Summers et al. (2008) found that hundreds of keV seed electron population, which can be further accelerated to MeV electrons (Horne et al., 2005; Thorne et al., 2013), is subject to rapid precipitation loss due to scattering by plume whistler mode waves, thus reducing the effect of MeV electron acceleration. In addition, plume whistler mode waves are

found to be capable of causing losses of energetic electrons with pitch angles closer to 90° (e.g., Li et al., 2007), which is a core population of energetic electrons in the radiation belts but is difficult to be scattered toward the loss cone by EMIC waves alone (Kersten et al., 2014; Usanova et al., 2014). In spite of the importance of plume whistler mode waves, it is crucial to note that the effects of plume whistler mode waves have not been accurately incorporated into most global radiation belt modeling yet (e.g., Albert et al., 2009; Glauert et al., 2014; Li et al., 2016; Ma et al., 2018; Tu et al., 2014). Therefore, we suggest that future radiation belt modeling efforts address the quantitative effects of plume whistler mode waves, as well as their combined scattering effects due to coexisting other types of magnetospheric waves, on the global evolution of energetic electron dynamics in the Earth's outer radiation belt.

Acknowledgments
This research is supported by the NSF grants AGS-1723588 and AGS-1847818, the NASA grants NNX17AD15G and NNX17AG07G, the AFOSR grant FA9550-15-1-0158, and the Alfred P. Sloan Research Fellowship FG-2018-10936. The research at The University of Iowa was supported by JHU/APL contract 921647 under NASA Prime contract NAS5-01072. The POES and MetOp data were obtained from https://www.ngdc.noaa.gov/stp/satellite/poes/. The Van Allen probes data from the EMFISIS instrument were obtained from http://emfisis.physics.uiowa.edu/Flight/. The Sym-H and AL indices were obtained from the OMNI data set (https://omniweb.gsfc.nasa.gov/ow.html).

References

Albert, J. M. (2002). Nonlinear interaction of outer zone electrons with VLF waves. *Geopysical Research Letters*, *29*(8), 1275. https://doi.org/10.1029/2001GL013941

Albert, J. M., Meredith, N. P., & Horne, R. B. (2009). Three-dimensional diffusion simulation of outer radiation belt electrons during the 9 October 1990 magnetic storm. *Journal of Geophysical Research*, *114*, A09214. https://doi.org/10.1029/2009JA014336

Borovsky, J. E., & Denton, M. H. (2008). A statistical look at plasmaspheric drainage plumes. *Journal of Geophysical Research*, *113*, A09221. https://doi.org/10.1029/2007JA012994

Borovsky, J. E., & Steinberg, J. T. (2006). The "calm before the storm" in CIR/magnetosphere interactions: Occurrence statistics, solar wind statistics, and magnetospheric preconditioning. *Journal of Geophysical Research*, *111*, A07S10. https://doi.org/10.1029/2005JA011397

Borovsky, J. E., Welling, D. T., Thomsen, M. F., & Denton, M. H. (2014). Long-lived plasmaspheric drainage plumes: Where does the plasma come from? *Journal of Geophysical Research: Space Physics*, *119*, 6496–6520. https://doi.org/10.1002/2014JA020228

Bortnik, J., Thorne, R. M., & Inan, U. S. (2008). Nonlinear interaction of energetic electrons with large amplitude chorus. *Geophysical Research Letters*, *35*, L21102. https://doi.org/10.1029/2008GL035500

Bortnik, J., Thorne, R. M., & Meredith, N. P. (2008). The unexpected origin of plasmaspheric hiss from discrete chorus emissions. *Nature*, *452*(7183), 62–66. https://doi.org/10.1038/nature06741

Burtis, W. J., & Helliwell, R. A. (1969). Banded chorus—A new type of VLF radiation observed in the magnetosphere by OGO 1 and OGO 3. *Journal of Geophysical Research*, *74*(11), 3002–3010. https://doi.org/10.1029/JA074i011p03002

Carpenter, D. L., Giles, B. L., Chappell, C. R., Décréau, P. M. E., Anderson, R. R., Persoon, A. M., et al. (1993). Plasmasphere dynamics in the duskside bulge region: A new look at an old topic. *Journal of Geophysical Research*, *98*(A11), 19,243–19,271. https://doi.org/10.1029/93JA00922

Chan, K.-W., & Holzer, R. E. (1976). ELF hiss associated with plasma density enhancements in the outer magnetosphere. *Journal of Geophysical Research*, *81*(13), 2267–2274. https://doi.org/10.1029/JA081i013p02267

Chen, A. J., & Wolf, R. A. (1972). Effects on the plasmasphere of a timevarying convection electric field. *Planetary and Space Science*, *20*(4), 483–509. https://doi.org/10.1016/0032-0633(72)90080-3

Chen, L., Thorne, R. M., Li, W., Bortnik, J., Turner, D., & Angelopoulos, V. (2012). Modulation of plasmaspheric hiss intensity by thermal plasma density structure. *Geophysical Research Letters*, *39*, L14103. https://doi.org/10.1029/2012GL052308

Elphic, R. C., Weiss, L. A., Thomsen, M. F., McComas, D. J., & Moldwin, M. B. (1996). Evolution of plasmaspheric ions at geosynchronous orbit during times of high geomagnetic activity. *Geophysical Research Letters*, *23*(16), 2189–2192. https://doi.org/10.1029/96GL02085

Evans, D. S., & Greer, M. S. (2004). *Polar Orbiting Environmental Satellite Space Environment Monitor-2: Instrument descriptions and archive data documentation archive data documentation. NOAA Tech. Mem. 93,* Version 1.4. Boulder, CO: Space Weather Predict. Cent.

Glauert, S. A., Horne, R. B., & Meredith, N. P. (2014). Three-dimensional electron radiation belt simulations using the BAS Radiation Belt Model with new diffusion models for chorus, plasmaspheric hiss, and lightning-generated whistlers. *Journal of Geophysical Research: Space Physics*, *119*, 268–289. https://doi.org/10.1002/2013JA019281

Goldstein, J., Sandel, B. R., Thomsen, M. F., Spasojevic, M., & Reiff, P. H. (2004). Simultaneous remote sensing and in situ observations of plasmaspheric drainage plumes. *Journal of Geophysical Research*, *109*, A03202. https://doi.org/10.1029/2003JA010281

Grebowsky, J. M. (1970). Model study of plasmapause motion. *Journal of Geophysical Research*, *75*(22), 4329–4333. https://doi.org/10.1029/JA075i022p04329

Green, J. C. (2013). *MEPED telescope data processing algorithm theoretical basis document*. Boulder, CO: Natl. Oceanic and Atmos. Admin. National Geophysical Data Center.

Hayakawa, M. Y., Tanaka, S. S., Sazhin, T. O., & Kurita, K. (1986). Characteristics of dawnside mid-latitude VLF emissions associated with substorms as deduced from the two-stationed direction finding measurement. *Planetary and Space Science*, *24*, 225–243.

Horne, R. B., Thorne, R. M., Shprits, Y. Y., Meredith, N. P., Glauert, S. A., Smith, A. J., et al. (2005). Wave acceleration of electrons in the Van Allen radiation belts. *Nature*, *437*(7056), 227–230. https://doi.org/10.1038/nature03939

Kennel, C. F., & Petschek, H. E. (1966). Limit on stably trapped particle fluxes. *Journal of Geophysical Research*, *71*(1), 1–28. https://doi.org/10.1029/JZ071i001p00001

Kersten, T., Horne, R. B., Glauert, S. A., Meredith, N. P., Fraser, B. J., & Grew, R. S. (2014). Electron losses from the radiation belts caused by EMIC waves. *Journal of Geophysical Research: Space Physics*, *119*, 8820–8837. https://doi.org/10.1002/2014JA020366

Kletzing, C. A., Kurth, W. S., Acuna, M., MacDowall, R. J., Torbert, R. B., Averkamp, T., et al. (2013). The Electric and Magnetic Field Instrument Suite and Integrated Science (EMFISIS) on RBSP. *Space Science Reviews*, *179*(1-4), 127–181. https://doi.org/10.1007/s11214-013-9993-6

Koons, H. C., & Roeder, J. L. (1990). A survey of equatorial magnetospheric wave activity between 5 and 8 R_E. *Planetary and Space Science*, *38*(10), 1335–1341. https://doi.org/10.1016/0032-0633(90)90136-E

Kurth, W. S., De Pascuale, S., Faden, J. B., Kletzing, C. A., Hospodarsky, G. B., Thaller, S., & Wygant, J. R. (2015). Electron densities inferred from plasma wave spectra obtained by the Waves instrument on Van Allen Probes. *Journal of Geophysical Research: Space Physics*, *120*, 904–914. https://doi.org/10.1002/2014JA020857

Li, W., Ma, Q., Thorne, R. M., Bortnik, J., Zhang, X. J., Li, J., et al. (2016). Radiation belt electron acceleration during the 17 March 2015 geomagnetic storm: Observations and simulations. *Journal of Geophysical Research: Space Physics*, *121*, 5520–5536. https://doi.org/10.1002/2016JA022400

Li, W., Ni, B., Thorne, R. M., Bortnik, J., Green, J. C., Kletzing, C. A., et al. (2013). Constructing the global distribution of chorus wave intensity using measurements of electrons by the POES satellites and waves by the Van Allen Probes. *Geophysical Research Letters*, *40*, 4526–4532. https://doi.org/10.1002/grl.50920

Li, W., Shprits, Y. Y., & Thorne, R. M. (2007). Dynamic evolution of energetic outer zone electrons due to wave-particle interactions during storms. *Journal of Geophysical Research*, *112*, A10220. https://doi.org/10.1029/2007JA012368

Li, W., Thorne, R. M., Bortnik, J., Reeves, G. D., Kletzing, C. A., Kurth, W. S., et al. (2013). An unusual enhancement of low-frequency plasmaspheric hiss in the outer plasmasphere associated with substorm-injected electrons. *Geophysical Research Letters*, *40*, 3798–3803. https://doi.org/10.1002/grl.50787

Li, W., Thorne, R. M., Bortnik, J., Shprits, Y. Y., Nishimura, Y., Angelopoulos, V., et al. (2011). Typical properties of rising and falling tone chorus waves. *Geophysical Research Letters*, *38*, L14103. https://doi.org/10.1029/2011GL047925

Ma, Q., Li, W., Bortnik, J., Thorne, R. M., Chu, X., Ozeke, L. G., et al. (2018). Quantitative evaluation of radial diffusion and local acceleration processes during GEM challenge events. *Journal of Geophysical Research: Space Physics*, *123*, 1938–1952. https://doi.org/10.1002/2017JA025114

Ma, Q., Li, W., Chen, L., Thorne, R. M., & Angelopoulos, V. (2014). Magnetosonic wave excitation by ion ring distributions in the Earth's inner magnetosphere. *Journal of Geophysical Research: Space Physics*, *119*, 844–852. https://doi.org/10.1002/2013JA019591

Mauk, B. H., Fox, N. J., Kanekal, S. G., Kessel, R. L., Sibeck, D. G., & Ukhorskiy, a A. (2013). Science objectives and rationale for the Radiation Belt Storm Probes mission. *Space Science Reviews*, *179*(1-4), 3–27. https://doi.org/10.1007/s11214-012-9908-y

Moldwin, M. B., Downward, L., Rassoul, H. K., Amin, R., & Anderson, R. R. (2002). A new model of the location of the plasmapause: CRRES results. *Journal of Geophysical Research*, *107*(A11), 1339. https://doi.org/10.1029/2001JA009211

Moldwin, M. B., Howard, J., Sanny, J., Bocchicchio, J. D., Rassoul, H. K., & Anderson, R. R. (2004). Plasmaspheric plumes: CRRES observations of enhanced density beyond the plasmapause. *Journal of Geophysical Research*, *109*, A05202. https://doi.org/10.1029/2003JA010320

Ni, B., Bortnik, J., Thorne, R. M., Ma, Q., & Chen, L. (2013). Resonant scattering and resultant pitch angle evolution of relativistic electrons by plasmaspheric hiss. *Journal of Geophysical Research: Space Physics*, *118*, 7740–7751. https://doi.org/10.1002/2013JA019260

Ni, B., Li, W., Thorne, R. M., Bortnik, J., Green, J. C., Kletzing, C. A., et al. (2014). A novel technique to construct the global distribution of whistler mode chorus wave intensity using low-altitude POES electron data. *Journal of Geophysical Research: Space Physics*, *119*, 5685–5699. https://doi.org/10.1002/2014JA019935

Ni, B., Thorne, R. M., Shprits, Y. Y., & Bortnik, J. (2008). Resonant scattering of plasma sheet electrons by whistler-mode chorus: Contribution to diffuse auroral precipitation. *Geophysical Research Letters*, *35*, L11106. https://doi.org/10.1029/2008GL034032

Omura, Y., Katoh, Y., & Summers, D. (2008). Theory and simulation of the generation of whistler-mode chorus. *Journal of Geophysical Research*, *113*, A04223. https://doi.org/10.1029/2007JA012622

Peck, E. D., Randall, C. E., Green, J. C., Rodriguez, J. V., & Rodger, C. J. (2015). POES MEPED differential flux retrievals and electron channel contamination correction. *Journal of Geophysical Research: Space Physics*, *120*, 4596–4612. https://doi.org/10.1002/2014JA020817

Rodger, C. J., Clilverd, M. A., Green, J. C., & Lam, M. M. (2010). Use of POES SEM-2 observations to examine radiation belt dynamics and energetic electron precipitation into the atmosphere. *Journal of Geophysical Research*, *115*, A04202. https://doi.org/10.1029/2008JA014023

Santolík, O., Gurnett, D. A., Pickett, J. S., Parrot, M., & Cornilleau-Wehrlin, N. (2003). Spatio-temporal structure of storm-time chorus. *Journal of Geophysical Research*, *108*(A7), 1278. https://doi.org/10.1029/2002JA009791

Santolik, O., Parrot, M., Storey, L. R. O., Pickett, J. S., & Gurnett, D. A. (2001). Propagation analysis of plasmaspheric hiss using Polar PWI measurements. *Geophysical Research Letters*, *28*(6), 1127–1130. https://doi.org/10.1029/2000GL012239

Shi, R., Li, W., Ma, Q., Green, A., Kletzing, C. A., Kurth, W. S., et al. (2019). Properties of whistler mode waves in Earth's plasmasphere and plumes. *Journal of Geophysical Research: Space Physics*, *124*. https://doi.org/10.1029/2018JA026041

Spasojević, M., Goldstein, J., Carpenter, D. L., Inan, U. S., Sandel, B. R., Moldwin, M. B., & Reinisch, B. W. (2003). Global response of the plasmasphere to a geomagnetic disturbance. *Journal of Geophysical Research*, *108*(A9), 1340. https://doi.org/10.1029/2003JA009987

Su, Z., Liu, N., Zheng, H., Wang, Y., & Wang, S. (2018). Large-amplitude extremely low frequency hiss waves in plasmaspheric plumes. *Geophysical Research Letters*, *45*(2), 565–577. https://doi.org/10.1002/2017GL076754

Summers, D., Ni, B., Meredith, N. P., Horne, R. B., Thorne, R. M., Moldwin, M. B., & Anderson, R. R. (2008). Electron scattering by whistler-mode ELF hiss in plasmaspheric plumes. *Journal of Geophysical Research*, *113*, A04219. https://doi.org/10.1029/2007JA012678

Summers, D., & Thorne, R. M. (2003). Relativistic electron pitch-angle scattering by electromagnetic ion cyclotron waves during geomagnetic storms. *Journal of Geophysical Research*, *108*(A4), 1143. https://doi.org/10.1029/2002JA009489

Tao, X., Bortnik, J., Albert, J. M., Thorne, R. M., & Li, W. (2014). Effects of discreteness of chorus waves on quasilinear diffusion-based modeling of energetic electron dynamics. *Journal of Geophysical Research: Space Physics*, *119*, 8848–8857. https://doi.org/10.1002/2014JA020022

Theodoridis, G. C., & Paolini, F. R. (1967). Pitch angle diffusion of relativistic outer belt electrons. *Annales de Geophysique*, *23*, 375.

Thorne, R. M., Li, W., Ni, B., Ma, Q., Bortnik, J., Baker, D. N., et al. (2013). Evolution and slow decay of an unusual narrow ring of relativistic electrons near L ~ 3.2 following the September 2012 magnetic storm. *Geophysical Research Letters*, *40*, 3507–3511. https://doi.org/10.1002/grl.50627

Thorne, R. M., Smith, E. J., Burton, R. K., & Holzer, R. E. (1973). Plasmaspheric hiss. *Journal of Geophysical Research*, *78*(10), 1581–1596. https://doi.org/10.1029/JA078i010p01581

Tsurutani, B. T., Falkowski, B. J., Pickett, J. S., Santolik, O., & Lakhina, G. S. (2015). Plasmaspheric hiss properties: Observations from Polar. *Journal of Geophysical Research: Space Physics*, *120*, 414–431. https://doi.org/10.1002/2014JA020518

Tsyganenko, N. A. (2002). A model of the near magnetosphere with a dawn-dusk asymmetry, 2, Parameterization and fitting to observations. *Journal of Geophysical Research*, *107*(A8), 1176. https://doi.org/10.1029/2001JA000220

Tu, W., Cunningham, G. S., Chen, Y., Morley, S. K., Reeves, G. D., Blake, J. B., et al. (2014). Event-specific chorus wave and electron seed population models in DREAM3D using the Van Allen Probes. *Geophysical Research Letters*, *41*, 1359–1366. https://doi.org/10.1002/2013GL058819

Usanova, M. E., Darrouzet, F., Mann, I. R., & Bortnik, J. (2013). Statistical analysis of EMIC waves in plasmaspheric plumes from Cluster observations. *Journal of Geophysical Research: Space Physics*, *118*, 4946–4951. https://doi.org/10.1002/jgra.50464

Usanova, M. E., Drozdov, A., Orlova, K., Mann, I. R., Shprits, Y., Robertson, M. T., et al. (2014). Effect of EMIC waves on relativistic and ultrarelativistic electron populations: Ground-based and Van Allen Probes observations. *Geophysical Research Letters*, *41*, 1375–1381. https://doi.org/10.1002/2013GL059024

Weiss, L., Lambour, R., Elphic, R., & Thomsen, M. (1997). Study of plasmaspheric evolution using geosynchronous observations and global modeling. *Geophysical Research Letters*, *24*(5), 599–602. https://doi.org/10.1029/97GL00351

Woodroffe, J. R., Jordanova, V. K., Funsten, H. O., Streltsov, A. V., Bengtson, M. T., Kletzing, C. A., et al. (2017). Van Allen probes observations of structured whistler mode activity and coincident electron Landau acceleration inside a remnant plasmaspheric plume. *Journal of Geophysical Research: Space Physics*, *122*, 3073–3086. https://doi.org/10.1002/2015JA022219

Yando, K., Millan, R. M., Green, J. C., & Evans, D. S. (2011). A Monte Carlo simulation of the NOAA POES Medium Energy Proton and Electron Detector instrument. *Journal of Geophysics Research*, *116*, A10231. https://doi.org/10.1029/2011JA016671

Zhang, W., Fu, S., Gu, X., Ni, B., Xiang, Z., Summers, D., et al. (2018). Electron scattering by plasmaspheric hiss in a nightside plume. *Geophysical Research Letters*, *45*, 4618–4627. https://doi.org/10.1029/2018GL077212

Zhu, H., Su, Z., Xiao, F., Zheng, H., Wang, Y., Shen, C., et al. (2015). Plasmatrough exohiss waves observed by Van Allen Probes: Evidence for leakage from plasmasphere and resonant scattering of radiation belt electrons. *Geophysical Research Letters*, *42*, 1012–1019. https://doi.org/10.1002/2014GL062964